Main Manuscript for

Mixed equilibrium/nonequilibrium effects govern surface mobility in polymer glasses

Jianquan Xu[a], Asieh Ghanekarade[b], Li Li[a], Huifeng Zhu[a], Hailin Yuan[c], Jinsong Yan[c], David S. Simmons[b,1], Ophelia K. C. Tsui[c,d,1], Xinping Wang[a,1]

[a]School of Chemistry and Chemical Engineering, Key Laboratory of Surface & Interface Science of Polymer Materials of Zhejiang Province, Zhejiang Sci-Tech University, Hangzhou 310018, China.

[b]Department of Chemical, Biological, and Materials Engineering, University of South Florida, Tampa, Florida 33620, United States.

[c]Department of Physics, Hong Kong University of Science and Technology, Hong Kong Special Administrative Region 999077, China.

[d]William Mong Institute of Nano Science and Technology, Hong Kong University of Science and Technology, Hong Kong Special Administrative Region 999077, China.

[1]To whom correspondence may be addressed. E-mail: dssimmons@usf.edu (DSS), okctsui@ust.hk (OKCT), or wxinping@zstu.edu.cn (XW).

Author contributions: X.W. and O.K.C.T. conceived and supervised the experiments; J.X., L.L., H.Z., H.Y., and J.Y. performed the experiments; and X.W., O.K.C.T., D.S.S., J.X., and L.L. analyzed experimental data. D.S.S. and A.G. conceived and analyzed the simulations; A.G. performed the simulations under the supervision of D.S.S. D.S.S., O.K.C.T., J.X., and X.W. wrote the original draft. All authors reviewed, edited, and agreed to publish the paper.

Competing Interest Statement: The authors may hold mutual funds and company stocks in their personal accounts, but it is believed that these holdings do not create conflicts of interests. The authors disclose research support as detailed in the Acknowledgements section.

Classification: Physical Sciences/Applied Physical Sciences

Keywords: glass transition, thin polymer film, surface dynamics, nanoconfinement

This PDF file includes:

Main Text
Figures 1 to 4

Abstract

Using angle-resolved X-ray photoelectron spectroscopy, sum-frequency generation vibrational spectroscopy, contact angle measurements, and molecular dynamics simulations, we verify that the glass transition temperature (T_g) of polymer glass is lower near the free surface. However, the experimental T_g-gradients showed a linear variation with depth (z) from the free surface, while the simulated equilibrium T_g-gradients exhibited a double exponential z-dependence. In typical simulations, T_g is determined based on the relaxation time of the system reaching a prescribed threshold value *at equilibrium*. Conversely, the experiments determined T_g by observing the unfreezing of molecular mobility during heating from a kinetically arrested, *non-equilibrium* glassy state. To investigate the impact of nonequilibrium effects on the T_g-gradient, we reduced the thermal annealing time in simulations, allowing the system to fall out of equilibrium. We observe a decrease in the relaxation time, and the emergence of a modified z-dependence consistent with a linear T_g-gradient near the free surface. We further validate the impact of non-equilibrium effects by studying the dependence of the T_g on the heating/cooling rate for polymer films of varying thickness (h). Our experimental results reveal significant variations in the T_g-heating/cooling rate dependence with h below the bulk T_g, which are also observed in simulation when the simulated system is not equilibrated. We explain our findings by the reduction in mass density within the inner region of the system under nonequilibrium conditions, as observed in simulation, and recent research indicating a decrease in the local T_g of a polymer when placed next to a softer material.

Significance Statement:

This study reveals a significant influence of nonequilibrium effects on the temperature dependent molecular relaxation times near the surface of polymer glasses. It also reveals qualitative alterations in the gradients of near-surface T_g and the T_g of thin polymer films due to these effects. The findings point to a new type of nonequilibrium phenomenon that occurs when there is strong spatial variation in T_g. This new phenomenon helps explain a puzzling 'onset' of strong interfacial effects around the bulk T_g. The results call for a reassessment of existing experimental data on nanoconfined glass films to consider these previously overlooked non-equilibrium effects, and suggest potential new insights into the physics of nanostructured polymers, including nanocomposites, films and block copolymers.

Main Text

Introduction

It has been established since the 1990s (1, 2) that the glass transition temperatures (T_g) of organic and polymer glass-formers can change upon confinement in domains ranging from the nanoscale (3-6) to the microscale (7, 8), depending on the method of investigation (9) and the rate or time-scale of measurement (10). These alterations have garnered significant attention. On the one hand, they play a central role in determining the properties (including viscosity (11), dielectric response (12), thermal expansivity (13, 14), and heat capacity (15)) of diverse nanostructured glasses (16), ranging from thin films to nanocomposites (17, 18) to block copolymers (19, 20) to semicrystalline polymers (21, 22). On the other hand, the study of changes in the glass transition caused by surface or finite size effects has long been anticipated to shed light on the nature of glass formation, which is a longstanding problem in condensed matter physics (23-25). However, progress has been hindered by the debate surrounding the propagation of surface-induced changes in dynamics and T_g into the material. While simulations have suggested that alterations in the mass density propagate over a distance of only ~1 nm (3, 4), additional results from the same simulation studies (3, 4) and experiments involving embedding of nanoparticles (5) or recovery of fluorescence from photobleached fluorescent molecules added to a polymer glass (6) have indicated longer propagation distances of several to ~10 nanometers. Other experiments, including those based on enthalpy recovery of polymer glass films on heating (7), T_g profiling by a local T_g-reporter (26), and mechanical relaxation measurements (8) have found even longer propagation distances of ~1 μm.

Over the past decade, molecular dynamics (MD) simulations have revealed the following coherent picture of alterations in dynamics near interfaces: The relaxation time (τ) of glasses exhibit a double exponential gradient form over ~10 nm from the surface (4, 27-30), the associated "dynamic T_g" takes on an exponential gradient form (29), and the temperature dependence of the near-surface relaxation time obeys a fractional power law decoupling relation with bulk. (Note that dynamic T_g's were determined based on the temperature at which τ reaches a prescribed value under *equilibrium* conditions. We refer to these T_g values as equilibrium T_g, or T_g^{eq}.) Experimental confirmation of these gradients has been suggested as a critical indicator of the nanoconfinement effect and could potentially reveal insights into the mechanism of the glass transition (29). However, there have been concerns about whether these gradient forms obtained from simulations, which are observed on relatively short timescales of ≤ ~100 ns, persist at experimental timescales of ~100 s during typical thermal T_g measurements. Several results suggest that this should not be a significant issue. For instance, simulations by Kob et al. (27) , Hocky et al. (28), and Vela et al. (31, 32) showed that the double-exponential mobility gradient saturates rather than continuing to evolve with increasing simulation times. Recent experiments by Li et al. (33) and Zhang et al. (34) also support the double-exponential form of the gradient of surface diffusivity in organic glasses and relaxation time in a colloidal glass, respectively.

Conventional experimental studies, including our own, measured thermal T_g using techniques such as differential scanning calorimetry (15) and dilatometry (or ellipsometry) (1). As these measurement schemes involve the system in a nonequilibrium state before or after the glass transition, we refer to these T_g values as nonequilibrium T_g (T_g^{ne}). Other experimental studies (11, 12, 35) use measurement schemes similar to simulations, monitoring dynamical

parameters such as τ (8, 12, 34, 35), viscosity (11), and diffusivity (33), as a function of temperature under isothermal equilibrium conditions or under quasi-equilibrium conditions during a *slow* temperature scan (with a rate < ~(30 K)*f* (43), where *f* is the frequency of an AC measurement) above the bulk T_g^{ne} ($T_{g,bulk}^{ne}$) (36) to determine T_g. These experiments, including those of Li et al. (33) and Zhang et al. (34) mentioned above were conducted above $T_{g,bulk}^{ne}$, and so measured equilibrium T_g^{eq}. Interestingly, T_g^{ne} and T_g^{eq} values obtained from the two different types of measurement schemes exhibit different thickness dependences in thin polymer films (9, 36), sparking a debate on whether nonequilibrium effects can alter or contribute to interfacial and nanoconfinement effects on T_g.

To test whether a corresponding exponential form of T_g gradient is also observed in experiments, we conducted measurements using three surface techniques with varying probe depths to determine the local nonequilibrium T_g as a function of depth (z) in various polymers. Our results reveal that $T_g^{ne}(z)$ gradients are linear in z. To gain a better understanding of our experimental result and the potential influence of nonequilibrium effects on the dynamics of nanoconfined glasses in general, we perform MD simulations on the dynamics of long-chain polymers, incorporating *extrinsic* nonequilibrium effects, associated with an initially nonequilibrium chain conformational state, and *intrinsic* nonequilibrium effects, which refer to the unavoidable loss of equilibrium at T_g^{ne}, to the systems. Results from these simulations not only explain the observed $T_g(z)$ gradient in our experiment, but also shed light on the puzzling "onset behavior" observed in experiments, where the temperature dependence of τ of polymer nanometer films qualitatively changes just below $T_{g,bulk}^{ne}$. Our findings suggest that nonequilibrium effects can significantly alter the relaxation time and T_g gradients near the surface of polymer glasses. Unintuitively, these modifications are more pronounced closer to the surface, despite the higher molecular mobility in this region that would suggest a faster attainment of equilibrium. To explain this unexpected behavior, we propose a nonequilibrium physical phenomenon that we observed in our simulation that is unique to glass systems possessing large interfacial dynamical gradients. Our findings provides insight into the dynamics of nanoconfined and nanostructured glasses and highlight the importance of considering nonequilibrium effects in future studies of these systems.

Results

To experimentally determine the $T_g^{ne}(z)$ profiles in cyclic PMMA (*c*-PMMA$_m$) and linear PMMA (*l*-PMMA$_m$) with varying degrees of polymerization (m), we have used a method some of us developed recently (37, 38). This method involves labeling the polymer with a fluoro-tracer and determining the temperature at which it gains mobility on heating, which is identified as T_g^{ne}. By using a combination of water contact angle measurements, sum-frequency generation vibrational spectroscopy, and X-ray photoelectron spectroscopy to finely adjust the measurement probe depth, z, we obtain the local T_g^{ne} at varying z with nanoscale resolution.

In Fig. 1, we present the $T_g^{ne}(z)$ data for the studied *c*-PMMA$_m$. The results indicate that beyond a depth of 1–2 nm from the surface, $T_g^{ne}(z)$ increases linearly with z until it reaches $T_{g,bulk}^{ne}$. The penetration depth, h_t (= 7.8 ± 1.2 nm), at which $T_{g,bulk}^{ne}$ is recovered is independent of molecular weight for the range of 12.9 to 27.9 kg/mol investigated, consistent with previous findings on the near-surface relaxation time of linear polystyrene (*l*-PS) (6). The observed linear gradient is also consistent with our *l*-PMMA data (see *SI Appendix*, Fig. S1) and published data

for *l*-PMMA (37) and *l*-PS (38). Our findings demonstrate that the experimentally measured $T_g^{ne}(z)$ differs from the exponential form observed for $T_g^{eq}(z)$ in simulations (29).

To determine whether this difference arises from nonequilibrium effects, we conduct simulations of glass formation in freestanding long-chain polymer films and their bulk counterpart upon incorporating both extrinsic and intrinsic nonequilibrium effects. To incorporate *extrinsic* nonequilibrium effects, we perform melt-quench simulations in which long-chain conformational statistics begin and remain modestly out of equilibrium. This approach qualitatively mimics the presence of trapped nonequilibrium chain configurations that are commonly produced during the fabrication of polymer films in a laboratory setting. To investigate *intrinsic* nonequilibrium effects at simulation timescales, we devise a simulation protocol to analyze changes in $T_g^{ne}(z)$ as the simulation time scale ($t_{ANN,max}$, the maximum annealing time applied to the system) varies. By comparing these results with $T_g^{eq}(z)$, we evaluate if nonequilibrium effects can explain the experimentally observed linear $T_g^{ne}(z)$.

To control the nonequilibrium effects, we employ a two-step protocol in our simulations. First, we subject the system to a high-temperature configurational annealing, where we control the extrinsic nonequilibrium effects. Then we thermally quench it to various measurement temperatures (T) and perform an isothermal (segmental) annealing for a maximum duration of $t_{ANN,max}$ to control the intrinsic nonequilibrium effects (see Simulation Method in *SI Appendix*). Consequently, the intrinsic system falls out of equilibrium when τ_{bulk}—the relaxation time in the middle of the film, which resembles bulk behavior—exceeds $t_{ANN,max}$. Therefore, $T_{g,bulk}^{ne}$ is approximately the temperature at which $\tau_{bulk} = t_{ANN,max}$. To maintain consistency, we define $T_{g,bulk}^{eq}$ as the temperature at which τ_{bulk} equals $t_{ANN,max}$ under equilibrium. In our simulation, $t_{ANN,max}$ is initially set to 10^6 Lennard-Jones time (τ_{LJ}). We measure τ at z from the intermediate scattering function of the polymers at z (see Simulation Method in *SI Appendix*). Fig. 2*A* displays the τ data obtained at several z's near the surface and in the middle of the film plotted versus $1/T$. Note that the relaxation time can only be inferred from relaxation functions that relax sufficiently within the observed time window. This explains the observed truncation of more low-temperature data for larger z values. Solid lines are fits of the equilibrium data, employing the vertical dotted line as a cutoff (ensuring that $\tau << t_{ANN,max}$) to the "Cooperative" functional form of Schmidtke et al. (39):

$$ln\,\tau = ln\,\tau_\infty + \frac{E_\infty}{T}\left\{1 + \exp\left[-\mu\left(\frac{T}{E_\infty} - \mathrm{d}\right)\right]\right\} \quad (1)$$

where τ_∞, E_∞, μ, and d are fit parameters. This equation has been demonstrated to accurately fit relaxation data and extrapolate equilibrium relaxation times to experimental timescales from computational data of shorter timescales (40). At lower temperatures, we thus continue to employ these fit curves (colored solid curves) to extrapolate the equilibrium dynamics at all the depths examined. Inside the midfilm, which emulates bulk behavior, the data (orange squares) closely obey the equilibrium line down to temperatures where τ is greater than $t_{ANN,max}$ (= 10^6 τ_{LJ}), showing that $T_{g,bulk}^{ne} \cong T_{g,bulk}^{eq}$, as found before (41). In the near-surface region ($z \leq 3.0625$), however, τ increasingly deviates from the equilibrium curves at low temperatures with decreasing z, with the onset of deviation occurring at shorter timescales (down to 10^4 τ_{LJ}). Indeed, these nonequilibrium effects apparently become pronounced at earlier timescales near the surface. Consistent with prior bulk simulations (41), dynamics in the midfilm remain equilibrium-like even well beyond the maximum annealing time of $t_{ANN,max} = 10^6$. However, upon approach to the

surface, the timescale of onset of pronounced downward deviations from expected equilibrium behavior (i.e., the commencement of a more Arrhenius dynamics regime) decreases. We note that while this onset appears to occur at lower temperature nearer the surface, this is merely due to the faster *equilibrium* dynamics in this region. These observations suggest that intrinsic nonequilibrium effects have a stronger impact on dynamics closer to the surface, where these effects tend to begin at a shorter timescale.

Similar to $T_{g,bulk}^{eq}$ and $T_{g,bulk}^{ne}$, we determine $T_g^{eq}(z)$ and $T_g^{ne}(z)$ by finding the temperatures where the equilibrium curves and nonequilibrium data, respectively, intersect the dotted line representing $\tau = 10^6\ \tau_{LJ}$ (= $t_{ANN,max}$) in Fig. 2*A*. In Fig. 2*B,* we compare the fractional change in $T_g^{ne}(z)$ and $T_g^{eq}(z)$ relative to $T_{g,bulk}^{eq}$. $T_g^{eq}(z)$ (filled squares) exhibits an exponential gradient, while the near-surface region of $T_g^{ne}(z)$ (orange circles) deviates significantly from an exponential form. Although the simulation's surface region is limited for determining its exact form, it aligns well with a linear gradient inspired by the reported experimental data reported above. When we decrease $t_{ANN,max}$ to $10^5\ \tau_{LJ}$, which is equivalent to decreasing the degree of supercooling or increasing the effective cooling rate (= $1/t_{ANN,max}$), this linear regime of the $T_g^{ne}(z)$ gradient (green diamonds) penetrates less far into the films, while $T_g^{eq}(z)$ (open squares) remains unchanged. In this simulation, $\tau = 10^6\ \tau_{LJ}$ corresponds to ~1 μs and the length scale of the bead-spring potential, $\sigma \approx 1$ nm. Since the penetration depth of $T_g^{ne}(z)$ grows with supercooling, a modest naïve linear extrapolation of the penetration depth vs. $\log(t_{ANN,max})$ suggests that the entire gradient would be linear by the experimental timescale at T_g^{ne}, which is consistent with our experimental results.

Our findings above provide insights into the source of the nonequilibrium effects. First, they cannot arise purely from *extrinsic* nonequilibrium (chain conformation) effects because nonequilibrium chain conformations exist above $T_{g,bulk}$, and yet our $T_g^{eq}(z)$ data continue to report an exponential gradient like that in prior simulations of short chains possessing conformational equilibrium (29). We further show in *SI Appendix*, Figs. S2 and S3 that improving chain conformational equilibrium weakens but does not eliminate deviations of τ from the equilibrium curves in the vicinity of T_g^{ne}. Therefore, it appears that the nonequilibrium effects found here are causally driven, to leading order, by the intrinsic loss of equilibrium near T_g^{ne}.

We note that the anomalous "onset behavior" of nanoconfined glasses mentioned in the introduction (10, 15, 42) also occurs near $T_{g,bulk}^{ne}$ in systems reported in the literature. With this in mind, we explore whether this onset can be attributed to nonequilibrium effects. We first reproduce this onset behavior by measuring the T_g of *l*-PMMA films with varying film thicknesses using ellipsometry and plotting the data as log (heating rate) versus $1/T_g^{ne}$ in Fig. 3*A* (various symbols). This figure is commonly interpreted as log ($1/\tau$) vs. $1/T$ (43) because the heating/cooling rate determines the minimum time for a system to regain or lose equilibrium during temperature ramping in conventional thermal T_g measurements. The temperatures where equilibrium is restored or lost are referred to as the thermal T_g for the respective heating/cooling rates. When the films were 76 nm thick and measured on heating at 100 or 50 K/min, their T_g^{ne} values matched the T_g^{ne} of the bulk polymer (the black line), indicating that they behave like bulk material. However, at temperatures below 392 K (≅ T_g^{bulk}; *SI Appendix,* Table S1), the data changes from the Vogel-Fulcher-Tammann (VFT) *T*-dependence, commonly exhibited by glasses, to an Arrhenius *T*-dependence. This crossover was also observed in PS (6, 8), and we believe it is because of the onset of nonequilibrium behaviors. As the film thickness decreased,

the data continued to follow an Arrhenius dependence, but it deviated more from the 76 nm data. This deviation can be explained by the existence of a gradient in τ and T_g, such that these quantities decrease as we move closer to the free surface of the film, as seen in Figs. 1 and 2. The most intriguing aspect of this figure is that the data of various film thicknesses extrapolate upward to a point on or near the bulk (black) curve.

To gain insight from simulation into whether this observation indeed emanates from nonequilibrium effects, we use a commonly accepted equivalence (43) between T_g^{ne} obtained during cooling and T_g^{eq} determined when the relaxation time threshold equals the reciprocal of the cooling rate times a constant (~30 K for typical polymers (43)). This suggests that Fig. 3*A* can be compared with a plot of log $(1/\tau)$ versus $1/T$. To generate data for this plot, we determine the simulated $\tau(z)$ at varying T and average them over supported films (on a dynamically non-perturbing substrate) of comparable thicknesses to yield the mean-film values of τ. To simulate $\tau(z)$ in equilibrium dynamics, we apply the empirically observed (and theoretically predicted (44)) double-exponential form for $\tau(z)$; in nonequilibrium dynamics, we introduce a linear region near the surface (as per *SI Appendix,* equation S8), with the extent of this region increasing linearly with $\log(t_{ANN,max})$. (See Section 2.2.7 of the SI for details.) Although the form of this linear region is crudely derived from only two time-points in Fig. 2*B*, it yields good consistency with experimental result when projected to experimental timescales, justifying its applications. In both cases, we employ equation (1) to extrapolate the bulk (midfilm) relaxation time to lower temperatures when needed, as is previously validated (40).

The obtained result, shown in Fig. 3*B*, reveals that the logarithmic rate vs. $1/T_g^{ne}$ data (dashed curves) exhibits an upward concavity that is absent in the equilibrium T_g^{eq} data (dotted curves). Mathematically, this is a qualitative consequence of the growing range of the linear nonequilibrium regime with increasing $t_{ANN,max}$ (or 1/(cooling rate)) (Fig. 2*B*). Practically, this leads to the emergence at low temperature of a regime of nearly Arrhenius dynamics. If we infer data points from these extrapolations over a timescale range and resolution comparable to various cooling-rate-T_g experiments (shown as solid circles in Fig. 3*B*), the results essentially replicate the onset behavior reported in Fig. 3*A*. Specifically, Arrhenius fits (colored solid lines) to these 'pseudodata' extrapolate upward towards a convergent point close to the equilibrium bulk (black) curve. In contrast, the T_g^{eq} (dotted) curves do not exhibit this convergence, but are projected to continue following the fractional power law decoupling behavior (31) previously reported in simulation and predicted in theory. While these curves exhibit an appreciable departure from the bulk curve, it is much weaker than that observed for the nonequilibrium curves. These observations suggest that the low temperature experimental onset behavior results from a linear gradient in T_g^{ne} caused by intrinsic nonequilibrium effects. The fact that the onset behavior has been observed in small molecule glasses (42), which lack the long-ranged and slow-relaxing conformational modes present in polymers (10), indicates that extrinsic nonequilibrium effects are not the causal origin of this onset behavior. Furthermore, this behavior is found whether T_g^{ne} is obtained by heating (Fig. 3*A*) or cooling (10, 42), which further reinforces the interpretation that intrinsic nonequilibrium effects are the main contributing factor to the onset behavior.

Discussion

Our observations suggest a unified picture of altered local relaxation times and glass transition temperature near a free surface. In equilibrium, surfaces induce an exponential T_g^{eq} gradient along with a weak long-ranged tail, which is consistent with the simulation literature (29) and experiments (33, 34). However, as the system falls out of equilibrium on cooling through T_g^{ne}, intrinsic nonequilibrium effects qualitatively modify and enhance the surface-induced gradient in T_g. A linear nonequilibrium gradient progressively grows inward from the surface with increasing equilibration timescale (or equivalently decreasing thermal quench rate), leading to an onset of much stronger and more Arrhenius (log (heating/cooling rate) vs. $1/T_g$) average-T_g shifts. It is this average-T_g shift that is probed in many experiments that report the onset of a new regime of behavior at low temperatures and rates.

Besides this onset behavior, there have been several other anomalous experimental observations that are based on T_g^{ne} measurements and could be affected by nonequilibrium phenomena. These include the observation of extraordinarily long-ranged T_g gradients at polymer-polymer interfaces (26) and reports of two-distinct T_g's in some thin films systems (45). Our results may suggest a new foundation for understanding these observations by adding nonequilibrium effects into consideration. Results of this work and two recent experiments (33, 34) suggest that the interfacial dynamical behavior observed in previous computer simulations (4, 27-29) likely represents the genuine equilibrium dynamical situation extended to experimental timescales and can be used to validate extant theories of glass transition (29) and shed light into the nature of the glass transition.

However, the mechanism by which intrinsic nonequilibrium effects produce deviations of τ^{ne} from the equilibrium counterpart (Fig. 2*A*) is counterintuitive. Specifically, the deviations are more pronounced closer to the surface even though the relaxation time in that region is shorter and equilibrium can be attained more rapidly. We suggest that intrinsic nonequilibrium effects may be driven by a non-local effect, which originates from a nonequilibrium density profile ($\rho(z)$) that emerges near the surface below $T_{g,bulk}^{ne}$ (46). Using simulations, we have obtained one such profile and presented it in Fig. 4*A* (blue diamonds). For comparison, the equilibrium profile is shown by orange circles. The nonequilibrium profile, obtained at $T = 0.35$, below $T_{g,bulk}^{ne}$ of ~0.4, displays a peak near the surface (at $z = 0$). These points are obtained based on linear fits to density over distinct temperature ranges above and below the local T_g, averaging over two surfaces, and then interpolating or extrapolating to $T = 0.35$. The error bars are 95% confidence intervals on the density obtained from these fits. Raw density data as a function of temperature can be found in Table S2. The underlying cause of this phenomenon can be seen in the temperature dependence of the equilibrium (liquid; orange line) and nonequilibrium (glassy; blue symbols and line) densities shown in Fig. 4*B*. When the temperature falls below $T_{g,bulk}^{ne}$, the midfilm (which resembles the bulk) begins to follow the weaker temperature dependence of the glass density (blue dashed line), reflecting a nonequilibrium decrease in density due to the vitrification of this bulk-like part of the film. As cooling continues below the bulk T_g, the density peak near the surface becomes more prominent, as inferred from the data of Fig. 4*B*.

This nonequilibrium effect cannot impact the midfilm T_g, because it emerges *below* the T_g of the midfilm (upon cooling) as a result of the loss of equilibrium at $T_{g,bulk}$ (~ 0.4). However, as shown in Fig. 4*A*, at their local T_g^{eq}, molecules just beneath the surface are sandwiched between the surface and a counterintuitively less dense and thus softer vitreous underlayer. Prior theory (44), experiment (26, 47), and simulation work (48) have indicated that nanoscale proximity to a soft domain tends to enhance molecular mobility. Therefore, in addition to the equilibrium effect

of a mobility enhancement by the free surface, these molecules also experience a nonequilibrium enhancement of mobility by their proximity to a softer underlayer. This leads to further suppression of T_g^{eq} beyond what would be expected from equilibrium dynamics. Moreover, since the relative softness of the underlayer driving this effect increases as the system is cooled more (see Fig. 4*B*), this additional mobility enhancement is more pronounced for material closer to the surface, which has a lower T_g even under equilibrium conditions. This explains why the nonequilibrium enhancement in mobility is most prominent near the free surface as shown in Fig. 2. In essence, this nonequilibrium effect amplifies the equilibrium dynamical gradient with an additional mobility-enhancing mechanism. However, because this mechanism is based on the underlying equilibrium dynamical enhancement present at the free surface, it would not occur without the underlying equilibrium (surface-induced mobility enhancing) effect in the first place.

Collectively, our results indicate that nonequilibrium effects play a central role in mediating the thermal and dynamical properties of thin film and nanostructured glasses. Furthermore, those properties can be modulated both by tuning the thermal pathway (and hence T_g^{ne}) or trapping nonequilibrium molecular conformations at high temperatures. These possibilities allow for new strategies to rationally control the properties of diverse nanostructured glasses. In this study, we have focused on novel nonequilibrium effects in freestanding films. However, our results suggest that these effects should emerge in the presence of any strong gradient in equilibrium relaxation time. We thus expect that these effects will play an important role in shaping the properties of other nanostructured polymers, including nanocomposites and semicrystalline polymers, which are of significant technological importance. In contrast, most current theories of altered dynamics near interfaces focus on purely equilibrium systems. Given the envisaged opportunities, it is crucial to prioritize extending these theories to account for nonequilibrium effects and exploring these effects in other technologically relevant nanostructured polymers in future research.

Materials and Methods

Linear (*l*-) and cyclic (*c*-) PMMA labeled with the fluoro group 2-perfluorooctylethyl methacrylate (FMA) were synthesized by combining atom transfer radical polymerization (ATRP) and copper (I)-catalyzed alkyne-azide cycloaddition (CuAAC) "click" reaction. The synthetic process is illustrated in *SI Appendix*, Fig. S4. The final products are *l*- and *c*-$PMMA_m$-b-FMA_n, confirmed by FTIR, NMR, and GPC (*SI Appendix*, Fig. S5), where *m* ranges from 129 to 279 and $n \leq 2$.

Water contact angle (WCA) was determined using a Krüss DSA-10 CA goniometer (Hamburg, Germany) by placing a ~2 μl drop of deionized water on the sample surface and allowing 3 s for the drop to stabilize before measurement. Sum frequency generation (SFG) spectra were obtained using a custom designed SFG spectrometer from EKSPLA in Lithuania. The incident angles of the tunable infrared (IR) laser beam and the 532 nm visible laser beam were set at 50° and 70°, respectively. The ssp (SF/*s*, visible/*s*, and IR/*p*) and IR/p polarization sum-frequency signals were collected at a wavenumber of 4 cm^{-1}, with *s* (*p*) indicating the polarization perpendicular (parallel) to the plane of incidence. Angle-resolved XPS spectra were obtained using a PHI5000C ESCA system equipped with an Al Kα X-ray source (1253.6 eV) running at 250 W and 140 kV. By adjusting the take-off angle (as shown in *SI Appendix*, Fig. S6*A*), the detection depth *z* can be varied from ~2.3–9.0 nm, with a resolution better than 1.2 nm. Considering that the penetration depths of WCA and SFG are 0.5 and1.0 nm, respectively, we

use WCA, SFG, and angle-resource XPS to monitor the change in the concentration of FMA with annealing temperature (T) across a range of z from 0.5–9.0 nm (refer to *SI Appendix*, Figs. S6*B* and S6*C*). From these data, we determine T_g^{ne} at various z as the temperature where the detection signal begins to increase with increasing T (refer to *SI Appendix*, Figs. S6*B* and S6*C*). For more detailed information on our experimental methods, please refer to the *SI Materials and Experimental Methods* section.

Our simulations investigate glass formation in freestanding model polymer films, focusing on analyzing both equilibrium and nonequilibrium T_g gradients. As detailed in the *SI Simulation Methods* section, we determined T_g^{ne} and T_g^{eq} in systems of bead-spring polymer films, with each polymer chain consisting of 400 or 1000 beads. In bead-spring simulations, polymer chains are typically initialized in an entropically unfavorable configuration and allowed to relax to equilibrium through an extended annealing period at a high temperature before thermally quenching the system towards T_g. To mimic the potential impact of extrinsic nonequilibrium effects associated with nonequilibrium chain conformations observed in experiments, we perform this high temperature annealing for a period slightly shorter than the chain reptation time. This duration is sufficient to alleviate highly tortuous configurations but not long enough to achieve full chain conformational equilibrium. In *SI Appendix*, Fig. S2, we show results for systems where chain conformations are annealed for longer periods, and in *SI Appendix*, Fig. S3 we show results obtained through a highly efficient Monte Carlo chain-rebridging protocol that yields a much faster equilibration of chain conformations. Both sets of results indicate that improving conformational equilibrium reduces, but does not completely eradicate, intrinsic nonequilibrium effects, namely, departures of τ from the equilibrium curves.

After the initial chain conformational annealing step, we subject the systems to thermal quenching from high temperature, with the configurations periodically saved at temperatures along the quench. Next, the configuration at temperature T is subjected to an isothermal annealing for a duration of 10 $\tau^{eq}(T)$, ensuring segmental equilibration at T. After this segmental annealing, dynamical data are gathered at each temperature during a data collection run. In our simulations, we set a maximum limit for the segmental annealing time, denoted by $t_{ANN,max}$. In our main simulations, this limit is set to 10^6 τ_{LJ}, where τ_{LJ} is the Lennard-Jones time unit. Just below the temperature T^* where $\tau^{eq}(T^*) = t_{ANN,max}$, the relaxation time surpasses the segmental annealing time, leading the system to deviate from equilibrium. Consequently, T^* is designated as T_g^{ne}, and the corresponding timescale for the nonequilibrium glass transition is $t_{ANN,max}$. To determine the local T_g^{ne} at a specific depth z, we define it as the temperature where the local segmental relaxation time τ at z surpasses $t_{ANN,max}$. The local T_g^{ne} at z is determined as the temperature where the equilibrium τ-T curve at z intersect $t_{ANN,max}$. As illustrated in Fig. 2*B,* the T_g^{ne}(z) profile is distinctly lower than the T_g^{eq}(z) profile. Decreasing $t_{ANN,max}$ to 10^6 τ_{LJ}, equivalent to increasing the effective cooling rate (=1/$t_{ANN,max}$) by a fact of 10, significantly reduces the degree of depression of T_g^{ne}(z) from T_g^{eq}(z). For more detailed simulation methods, please refer to the *SI Simulation Methods* section.

Acknowledgments

JX, XW, OKCT, DSS, and AG would like to express their gratitude for the funding support received for their research. JX and XW were supported by the National Natural Science Foundation of China (grants 22161160317, 22203075, and 22173081). OKCT received support from the Research Grants Council of Hong Kong (grant N_HKUST623/21). DSS and AG were supported by the United States National Science Foundation CBET Program (grant 2208238).

References

1. J. L. Keddie, R. A. L. Jones, R. A. Cory, Interface and Surface Effects on The Glass-Transition Temperature in Thin Polymer Films. *Faraday Discuss.* **98**, 219-230 (1994).
2. C. L. Jackson, G. B. McKenna, The glass transition of organic liquids confined to pores. *J. Non-Cryst. Solids* **131-133**, 221-224 (1991).
3. Y. Zhou, S. T. Milner, Short-Time Dynamics Reveals Tg Suppression in Simulated Polystyrene Thin Films. *Macromolecules* **50**, 5599-5610 (2017).
4. W. Zhang, F. W. Starr, J. F. Douglas, Activation free energy gradient controls interfacial mobility gradient in thin polymer films. *J. Chem. Phys.* **155**, 174901 (2021).
5. J. H. Teichroeb, J. A. Forrest, Direct Imaging of Nanoparticle Embedding to Probe Viscoelasticity of Polymer Surfaces. *Phys. Rev. Lett.* **91**, 016104 (2003).
6. K. Paeng, S. F. Swallen, M. D. Ediger, Direct Measurement of Molecular Motion in Freestanding Polystyrene Thin Films. *J. Am. Chem. Soc.* **133**, 8444-8447 (2011).
7. V. M. Boucher, D. Cangialosi, A. Alegria, J. Colmenero, Enthalpy Recovery in Nanometer to Micrometer Thick Polystyrene Films. *Macromolecules* **45**, 5296-5306 (2012).
8. H. Yuan, J. Yan, P. Gao, S. K. Kumar, O. K. C. Tsui, Microscale mobile surface double layer in a glassy polymer. *Sci. Adv.* **8**, eabq5295 (2022).
9. M. D. Ediger, J. A. Forrest, Dynamics near Free Surfaces and the Glass Transition in Thin Polymer Films: A View to the Future. *Macromolecules* **47**, 471-478 (2014).
10. Z. Fakhraai, J. A. Forrest, Probing slow dynamics in supported thin polymer films. *Phys. Rev. Lett.* **95**, 025701 (2005).
11. Z. Yang, Y. Fujii, F. K. Lee, C.-H. Lam, O. K. C. Tsui, Glass Transition Dynamics and Surface Layer Mobility in Unentangled Polystyrene Films. *Science* **328**, 1676-1679 (2010).
12. K. Fukao, Y. Miyamoto, Slow dynamics near glass transitions in thin polymer films. *Phys. Rev. E* **64**, 011803 (2001).
13. S. Kawana, R. A. L. Jones, Character of the Glass Transition in Thin Supported Polymer Films. *Phys. Rev. E* **63**, 021501 (2001).
14. T. Miyazaki, K. Nishida, T. Kanaya, Contraction and reexpansion of polymer thin films. *Phys. Rev. E* **69**, 022801 (2004).
15. S. Gao, Y. P. Koh, S. L. Simon, Calorimetric Glass Transition of Single Polystyrene Ultrathin Films. *Macromolecules* **46**, 562-570 (2013).
16. D. S. Simmons, An Emerging Unified View of Dynamic Interphases in Polymers. *Macromol. Chem. Phys.* **217**, 137-148 (2016).
17. F. W. Starr, J. F. Douglas, D. Meng, S. K. Kumar, Bound Layers “Cloak” Nanoparticles in Strongly Interacting Polymer Nanocomposites. *ACS Nano* **10**, 10960-10965 (2016).
18. S. Cheng, B. Carroll, V. Bocharova, J.-M. Carrillo, B. G. Sumpter, A. P. Sokolov, Focus: Structure and dynamics of the interfacial layer in polymer nanocomposites with attractive interactions. *J. Chem. Phys.* **146**, 203201 (2017).
19. D. Christie, R. A. Register, R. D. Priestley, Direct Measurement of the Local Glass Transition in Self-Assembled Copolymers with Nanometer Resolution. *ACS Central Science* **4**, 504-511 (2018).
20. C. B. Roth, J. M. Torkelson, Selectively Probing the Glass Transition Temperature in Multilayer Polymer Films: Equivalence of Block Copolymers and Multilayer Films of Different Homopolymers. *Macromolecules* **40**, 3328-3336 (2007).
21. B. Wunderlich, Reversible crystallization and the rigid–amorphous phase in semicrystalline macromolecules. *Prog. Polym. Sci.* **28**, 383-450 (2003).
22. J. Lee, J. H. Mangalara, D. S. Simmons, Correspondence between the rigid amorphous fraction and nanoconfinement effects on glass formation. *J. Polym. Sci., Part B: Polym. Phys.* **55**, 907-918 (2017).
23. P. W. Anderson, Through the Glass Lightly. *Science* **267**, 1615-1616 (1995).
24. P. G. Debenedetti, F. H. Stillinger, Supercooled liquids and the glass transition. *Nature* **40**, 259-267 (2001).
25. K. Chang, The Nature of Glass Remains Anthing but Clear. *New York Times* (July 29, 2008) .
26. R. R. Baglay, C. B. Roth, Local glass transition temperature Tg(z) of polystyrene next to different polymers: Hard vs. soft confinement. *J. Chem. Phys.* **146**, 203307 (2017).

27. W. Kob, S. Roldán-Vargas, L. Berthier, Non-monotonic temperature evolution of dynamic correlations in glass-forming liquids. *Nat. Phys.* **8**, 164-167 (2012).
28. G. M. Hocky, L. Berthier, W. Kob, D. R. Reichman, Crossovers in the dynamics of supercooled liquids probed by an amorphous wall. *Phys. Rev. E* **89**, 052311 (2014).
29. K. S. Schweizer, D. S. Simmons, Progress towards a phenomenological picture and theoretical understanding of glassy dynamics and vitrification near interfaces and under nanoconfinement. *J. Chem. Phys.* **151**, 240901 (2019).
30. Z. Hao, A. Ghanekarade, N. Zhu, K. Randazzo, D. Kawaguchi, K. Tanaka, X. Wang, D. S. Simmons, R. D. Priestley, B. Zuo, Mobility gradients yield rubbery surfaces on top of polymer glasses. *Nature* **596**, 372-376 (2021).
31. D. Diaz-Vela, J.-H. Hung, D. S. Simmons, Temperature-Independent Rescaling of the Local Activation Barrier Drives Free Surface Nanoconfinement Effects on Segmental-Scale Translational Dynamics near Tg. *ACS Macro Lett.* **7**, 1295-1301 (2018).
32. D. Diaz Vela, A. Ghanekarade, D. S. Simmons, Probing the Metrology and Chemistry Dependences of the Onset Condition of Strong "Nanoconfinement" Effects on Dynamics. *Macromolecules* **53**, 4158-4171 (2020).
33. Y. Li, W. Zhang, C. Bishop, C. Huang, M. D. Ediger, L. Yu, Surface diffusion in glasses of rod-like molecules posaconazole and itraconazole: effect of interfacial molecular alignment and bulk penetration. *Soft Matter* **16**, 5062 (2020).
34. Q. Zhang, W. Li, K. Qiao, Y. Han, Surface premelting and melting of colloidal glasses. *Sci. Adv.* **9**, eadf1101 (2023).
35. P. G. Santangelo, C. M. Roland, Molecular weight dependance of fragility in polystyrene. *Macromolecules* **31**, 4581-4585 (1998).
36. R. D. Priestley, D. Cangialosi, S. Napolitano, On the equivalence between the thermodynamic and dynamic measurements of the glass transition in confined polymers. *J. Non-Cryst. Solids* **407**, 288-295 (2015).
37. B. Zuo, Y. Liu, L. Wang, Y. Zhu, Y. Wang, X. Wang, Depth Profile of the Segmental Dynamics at a Poly(methyl methacrylate) Film Surface. *Soft Matter* **9**, 9376-9384 (2013).
38. C. Zhang, L. Li, J. Chen, Y. Yang, B. Zuo, J. Li, X. Wang, Chemical Structure Dependence of Surface Layer Thickness on Polymer Films. *J. Phys. Chem. C* **124**, 12448-12456 (2020).
39. B. Schmidtke, M. Hofmann, A. Lichtinger, E. A. Rössler, Temperature Dependence of the Segmental Relaxation Time of Polymers Revisited. *Macromolecules* **48**, 3005-3013 (2015).
40. J.-H. Hung, T. K. Patra, D. S. Simmons, Forecasting the experimental glass transition from short time relaxation data. *J. Non-Cryst. Solids* **544**, 120205 (2020).
41. J.-H. Hung, T. K. Patra, V. Meenakshisundaram, J. H. Mangalara, D. S. Simmons, Universal localization transition accompanying glass formation: insights from efficient molecular dynamics simulations of diverse supercooled liquids. *Soft Matter* **15**, 1223-1242 (2019).
42. Y. Zhang, E. C. Glor, M. Li, T. Liu, K. Wahid, W. Zhang, R. A. Riggleman, Z. Fakhraai, Long-range correlated dynamics in ultrathin molecular glass films. *J. Chem. Phys.* **145**, 114502 (2016).
43. J. E. K. Schawe, Vitrification in a wide cooling rate range: The relations between cooling rate, relaxation time, transition width, and fragility. *J. Chem. Phys.* **141**, 184905 (2014).
44. A. D. Phan, K. S. Schweizer, Theory of the spatial transfer of interface-nucleated changes of dynamical constraints and its consequences in glass-forming films. *J. Chem. Phys.* **150**, 044508 (2019).
45. J. E. Pye, C. B. Roth, Two Simultaneous Mechanisms Causing Glass Transition Temperature Reductions in High Molecular Weight Freestanding Polymer Films as Measured by Transmission Ellipsometry. *Phys. Rev. Lett.* **107**, 235701 (2011).
46. J. H. Mangalara, M. D. Marvin, D. S. Simmons, Three-Layer Model for the Emergence of Ultrastable Glasses from the Surfaces of Supercooled Liquids. *J. Phys. Chem. B* **120**, 4861-4865 (2016).
47. R. R. Baglay, C. B. Roth, Communication: Experimentally Determined Profile of Local Glass Transition Temperature across a Glassy-Rubbery Polymer Interface with a Tg Difference of 80 K. *J. Chem. Phys.* **143**, 111101 (2015).
48. R. J. Lang, W. L. Merling, D. S. Simmons, Combined Dependence of Nanoconfined Tg on Interfacial Energy and Softness of Confinement. *ACS Macro Lett.* **3**, 758-762 (2014).

Figures

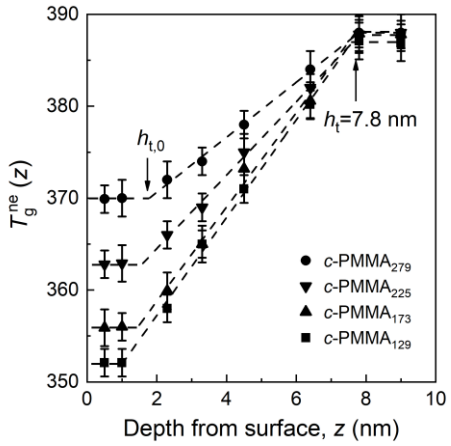

Fig. 1. Experimental depth profiles $T_g^{ne}(z)$ taken at the surface of various *c*-PMMA polymers. Dashed lines are the best fits to a linear gradient with details of the fits reported in *SI Appendix*, Table S3.

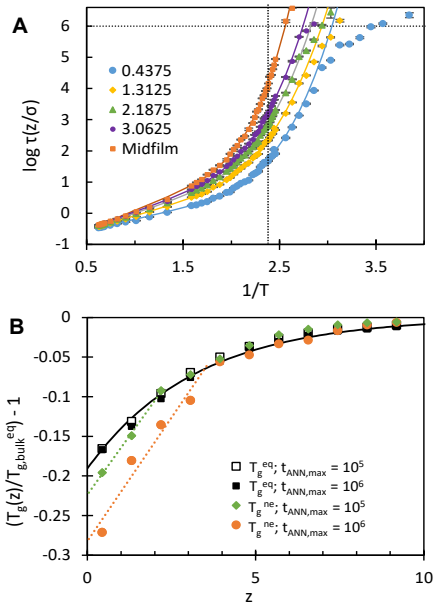

Fig. 2. Simulation results revealing intrinsic nonequilibrium effects on near-surface τ(z) of long-chain films. (*A*) Segmental relaxation time τ vs. inverse temperature for various segmental layers at different distances z/σ from the surface, as given by the legend (σ is the length scale of the bead-spring potential). The dotted lines represent the low-temperature cutoff for inclusion of equilibrium relaxation time data and $\tau = t_{ANN,max} = 10^6$. The curved lines show fits of the data to an established model for equilibrium dynamics (40). Deviations from the curved equilibrium lines to the right of the vertical dotted line indicate intrinsic nonequilibrium effects on the near-surface relaxation time near and below $T_{g,bulk}^{eq}$. (*B*) Normalized alteration gradients of T_g^{eq} and T_g^{ne} relative to bulk for systems with $t_{ANN,max} = 10^5$ and 10^6 (inicated in the legend). The solid line shows a fit of T_g^{eq} (z) to an exponential gradient form to the T_g^{eq} data, while the dotted lines (in corresponding colors) represent linear fits to the surface region where T_g^{ne} deviates significantly from T_g^{eq}.

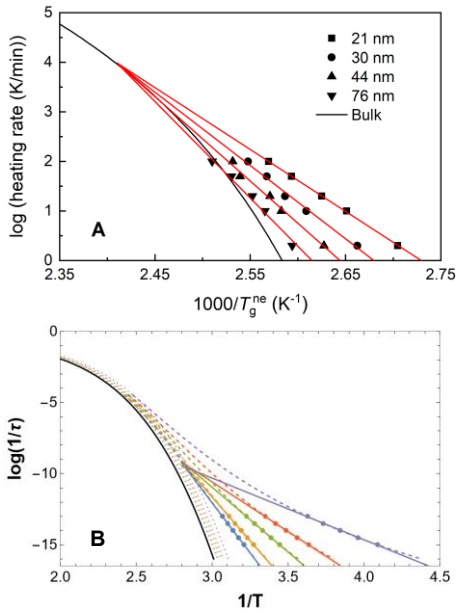

Fig. 3. Experimental and simulation data showing the onset behavior of log (heating rate) or log (1/τ) vs. $1/T_g^{ne}$ in polymer nanofilms. (*A*) Experimental analysis of mean-film T_g^{ne} for *l*-$PMMA_{173}$ films of varying thicknesses (indicated in the legend) and heating rates. The red lines represent fits to Arrhenius rate laws, extrapolating upwards to an intercept near the equilibrium bulk curve (solid black line), similar to prior T_g^{ne} measurements conducted during cooling. (*B*) Simulated results on mean logarithmic relaxation rate log(1/τ) for a supported film on a dynamically neutral substrate plotted vs. $1/T$, for comparison to experimental data. (See the supporting Simulation Method for details) Dashed lines show predicted behavior for mean-film T_g^{ne} with different thicknesses (h = 20 σ, 30 σ, 40 σ, 60 σ, and 75 σ—top to bottom), while dotted lines show predicted behavior of T_g^{eq} for the same systems. Points represent "pseudodata" mimicking T_g^{eq} data that could be obtained in experiment, along with solid lines passing through them representing Arrhenius fits. These lines extrapolate upwards to a point near the equilibrium bulk curve.

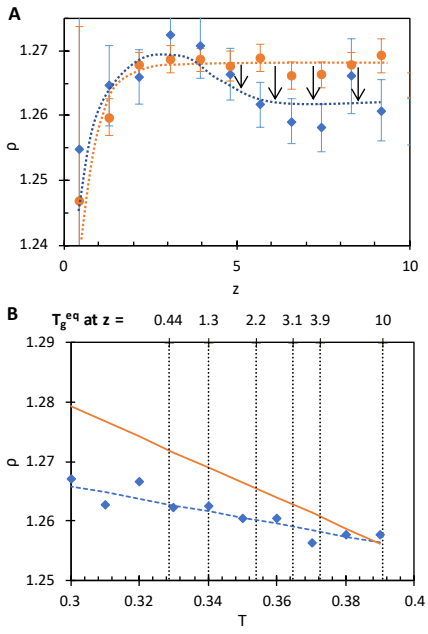

Fig. 4. Illustrating the proposed relationship between nonequilibrium density gradient effects and nonequilibrium T_g gradient effects. (*A*) Nonequilibrium glassy density (blue diamonds) and equilibrium liquid density extrapolated from high-temperature melt data (orange circles) vs. distance (in units of σ) from the film surface at a simulation temperature of ~0.35, which is below the system's bulk T_g of ~0.4. Dotted lines are guides-to-the-eye. The nonequilibrium suppression in ρ in the vitreous interior is beyond uncertainty. This region is posited to serve as a soft, T_g-reducing underlayer at temperatures below the interior T_g, driving a further nonequilibrium reduction of the T_g of the near-surface material at still lower temperatures. (*B*) Temperature dependence of the extrapolated equilibrium density (orange line) and of the nonequilibrium, glassy state density of the film interior below the bulk T_g (blue diamonds and dashed guide-to-the-eye line). The vertical dotted lines correspond to nonequilibrium local T_g values at distances from the surface, as labeled at the top of the panel. The length of the arrows in panel *A*, showing nonequilibrium suppression in density in the film interior, corresponds to the difference between the two lines in panel *B*. This difference grows on cooling, resulting in a larger difference at the local T_g nearer the surface. Consequently, a relatively softer (and more T_g-suppressing) underlayer material is present nearer the surface.